JOURNAL OF PROPULSION AND POWER
Vol. 24, No. 4, July–August 2008

Complex Wall Injector Array for High-Speed Combustors

Joseph A. Schetz,* Luca Maddalena,† and Ryan Throckmorton‡
Virginia Polytechnic Institute and State University, Blacksburg, Virginia 24061-0203
and
Reece Neel§
AeroSoft, Inc., Blacksburg, Virginia 24060

DOI: 10.2514/1.36660

This paper presents the results of experimental and numerical studies of an array of injectors combining inclined circular and diamond-shaped sonic nozzles for application to high-Mach-number airbreathing vehicles with light-gas fuels. The freestream Mach number was 4, and helium was used as the injectant to safely simulate hydrogen fuel. The diamond injector provided improvements in penetration of more than a factor of 2, compared with the circular injectors. This is a greater increase than had been inferred earlier by comparing test results with isolated diamond and circular injectors. The rate of mixing as indicated by the decay of maximum concentration in the plume was about the same. Computational fluid dynamics with a Reynolds-averaged Navier–Stokes formulation was applied to this flow problem with four different turbulence models. The helium-mixing predictions from the four turbulence models showed that the simulations are heavily impacted by the turbulence model selection. None of the turbulence models were able to accurately simulate the helium mixing shown in the experiment, but some models did much better than others. From the selected models, the Wilcox k-ω model had the best correlation with the experimental helium-concentration profiles. The computational fluid dynamic solutions were also probed to elucidate the behavior of the flow in the plumes from the circular and diamond injectors. From a design point of view, these results show that it is useful to combine inclined diamond and circular injectors to achieve good fuel coverage and fuel/air mixing across a combustor.

Nomenclature

C_d	=	discharge coefficient
d	=	jet diameter
d_{eff}	=	effective diameter
G_j	=	injectant mass flow rate per injector
M	=	Mach number
P	=	pressure
$\bar{q}$	=	jet-to-freestream momentum-flux ratio
R_b	=	effective radius per injector
T	=	temperature
x	=	axial distance downstream of injector center
y	=	lateral distance from the injector centerline
y^+	=	vertical distance in wall units
z	=	vertical distance from the wall
ω	=	vorticity

Subscripts

j	=	jet-exit property
t	=	total condition
∞	=	freestream property

Presented as Paper 105 at the 46th AIAA Aerospace Sciences Meeting and Exhibit, Reno, NV, 10 January 2008; received 14 January 2008; accepted for publication 16 April 2008.

*Holder of the Fred D. Durham Chair, Aerospace and Ocean Engineering Department. Fellow AIAA.

†Graduate Research Assistant, Aerospace and Engineering Department; currently Postdoctoral Fellow, California Institute of Technology. Student Member AIAA.

‡Graduate Research Assistant, Aerospace and Ocean Engineering Department. Student Member AIAA.

§Research Engineer. Member AIAA.

I. Introduction

AS A result of the very high freestream velocity of airbreathing vehicles operating in the range of Mach 10, fuel residence time is on the order of milliseconds [1], and efficient supersonic combustion presents a challenge. It is therefore desirable to enhance penetration and mixing of the fuel plume to accomplish rapid combustion, leading to a reduction of the required combustor length, reducing the skin-friction drag and heat transfer and increasing the net thrust. To improve the overall engine efficiency, the injection process must also induce low total pressure losses. Jet injector enhancement in high-speed flows also has applications in other fields such as thermal protection systems and vehicle control by jet thrusters.

Many injector configurations have been studied by various groups in an attempt to produce enhanced mixing and penetration in wall injectors. Some of these configurations can be seen in Fig. 1, including swept ramps [1–10], slot injectors [11,12], transverse injection [13–18], and jet swirl [19–24]. An extensive review of injector mixing characteristics is given in Schetz et al. [25]. The focus of the current investigation is flush-wall injectors. Flush-wall injectors are often preferred over in-stream injectors such as ramps or struts because they minimize total pressure losses and heating. Wall injectors produce a counter-rotating vortex pair [26] when they interact with the freestream crossflow, and this is the major method of mixing enhancement in these injectors, compared with coaxial jets.

One of the more successful studies in enhancing jet flow penetration in single-hole injectors was the use of a wedge-shaped hole with a rounded back, introduced by Barber et al. [13]. See the sketch in the middle of Fig. 1. The wedge-shaped front of the hole mitigated boundary-layer separation upstream of the jet, resulting in higher penetration than with round injectors. The major drawback of the wedge injector design was that separation still occurred downstream of the injector due to the rounded back. Tomioka et al. [14] showed that replacing the round back of the injector hole with a rear-facing wedge would help to negate this problem. See the sketch in the middle of the bottom row in Fig. 1. The more recent work on diamond injectors of Grossman et al. [27] extended the results of Tomioka et al. [14] to higher air Mach numbers and light-gas injection.

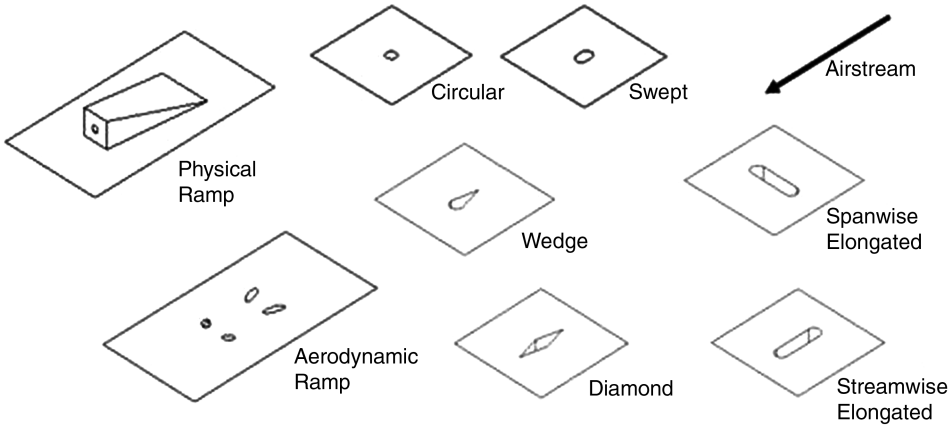

Fig. 1 Examples of various injector configurations.

The purpose of the present research is to investigate the effectiveness of combining low-angled diamond injectors and circular injectors into an array. The idea is to try to capture the best features of diamond and circular injectors and perhaps also achieve some synergism. The nominal Mach 4 airflow simulates conditions that a combustor would encounter in Mach 10 flight. Helium was used to safely simulate hydrogen. There are two main objectives of a cold-flow mixing study such as conducted here. The first objective is to assess the penetration and mixing of the simulated fuel injectors in comparison with the expectations upon which the injector arrangement was designed. The second objective is to quantify the uncertainty of computational fluid dynamics (CFD) predictions for such an injector design so that the reliability of CFD predictions for hot-flow combusting conditions can be judged. Detailed experimental flowfield studies are extremely challenging under the hot-flow conditions of interest for Mach 10 vehicles, and so the combustor designer must rely on CFD.

II. Experimental Methods

A. Test Facility

These experiments were conducted in the Virginia Polytechnic Institute and State University (VT) blowdown-type supersonic wind tunnel shown in Fig. 2.

The supersonic wind-tunnel setup for the experiments used a converging–diverging nozzle to achieve a nominal Mach 4 flow in the test section. Flow conditions involved total pressure and temperature in the plenum chamber of $P_{t,\text{plenum}} = 1034$ kPa and $T_{t,\text{plenum}} = 295$ K. However, there was a weak oblique shock observed at the end of the nozzle where the floor plate attached, resulting in actual freestream conditions of Mach number $M_\infty = 3.8$, total pressure $P_{t,\infty} = 1029$ kPa, and total temperature $T_{t,\infty} = 295$ K at the injection station. The turbulent boundary-layer thickness at the injection station was determined from schlieren photographs to be 17 mm.

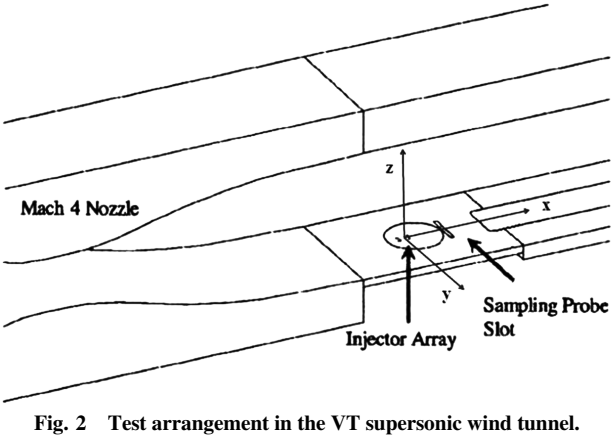

Fig. 2 Test arrangement in the VT supersonic wind tunnel.

B. Data Acquisition

Data from the experiments were acquired using a 16-channel, 16-bit A/D converter. A 64-channel multiplexer with a built-in cold-junction compensator was used for temperature measurements with a sampling rate of 500 Hz. LabVIEW was used both to control the wind tunnel, traverse system, and injection and to collect data from the measurement probes.

C. Injectors

Helium was used in these experiments to safely simulate hydrogen fuel. When comparing injectors, it is important to normalize data to provide an objective and accurate comparison. Often, injector diameter is used to normalize lengths for round injectors of varying sizes. It is common to include a discharge coefficient into an effective diameter: $d_{\text{eff}} = C_d^{1/2} d$. However, when comparing injectors of different shapes, effective diameter can be a poor length scale, because changing injection properties can affect some shapes differently than others. For such cases, a useful alternative length scale is the effective radius R_b, defined as follows [13]:

$$R_b = \sqrt{\frac{G_j}{\rho_\infty u_\infty}} \tag{1}$$

To fully describe injector conditions, another parameter is used, called the jet-to-freestream momentum-flux ratio $\bar{q}$, defined as follows:

$$\bar{q} = \frac{(\rho u^2)_j}{(\rho u^2)_\infty} = \frac{(p\gamma M^2)_j}{(p\gamma M^2)_\infty} \tag{2}$$

The injector insert for the experimental arrangement is shown in Fig. 3. The center diamond injector has circular injectors on either side, and thin splitter plates are located to the outside of the round-hole injectors to simulate a periodic array. This injector insert fits into the floor plate of the VT supersonic wind tunnel, as shown in Fig. 4, with the sampling probe mounted behind. The test conditions are as follows: The freestream conditions are $M_a = 3.8$, $T_{ta} = 295$ K, and $P_{ta} = 1029$ kPa. The test helium-jet conditions are three 30-deg jets (two circular, 1 diamond), $M_j = 1$, $T_{tj} = 295$ K, $P_{tj,\text{circular}} = 375$ kPa, $P_{tj,\text{diamond}} = P_{tj,\text{circular}}/4$, G_j per injector $= 0.322$ gm/s, $\bar{q}_{\text{diamond}} = 0.5$, $\bar{q}_{\text{circular}} = 2.0$, $d = 1.074$ mm, $d_{\text{eff}} = 1.058$ mm, $R_b = 1.09$ mm, $A_{j,\text{diamond}} = 4A_{j,\text{circular}}$, and distance between injectors$/d = 10$.

The diamond injector has a greater exit area and lower injection pressure to match the mass flow rate from the circular injectors. A lower injection pressure, and thus lower $\bar{q}_{\text{diamond}}$, has proven desirable for diamond injectors, compared with round injectors,

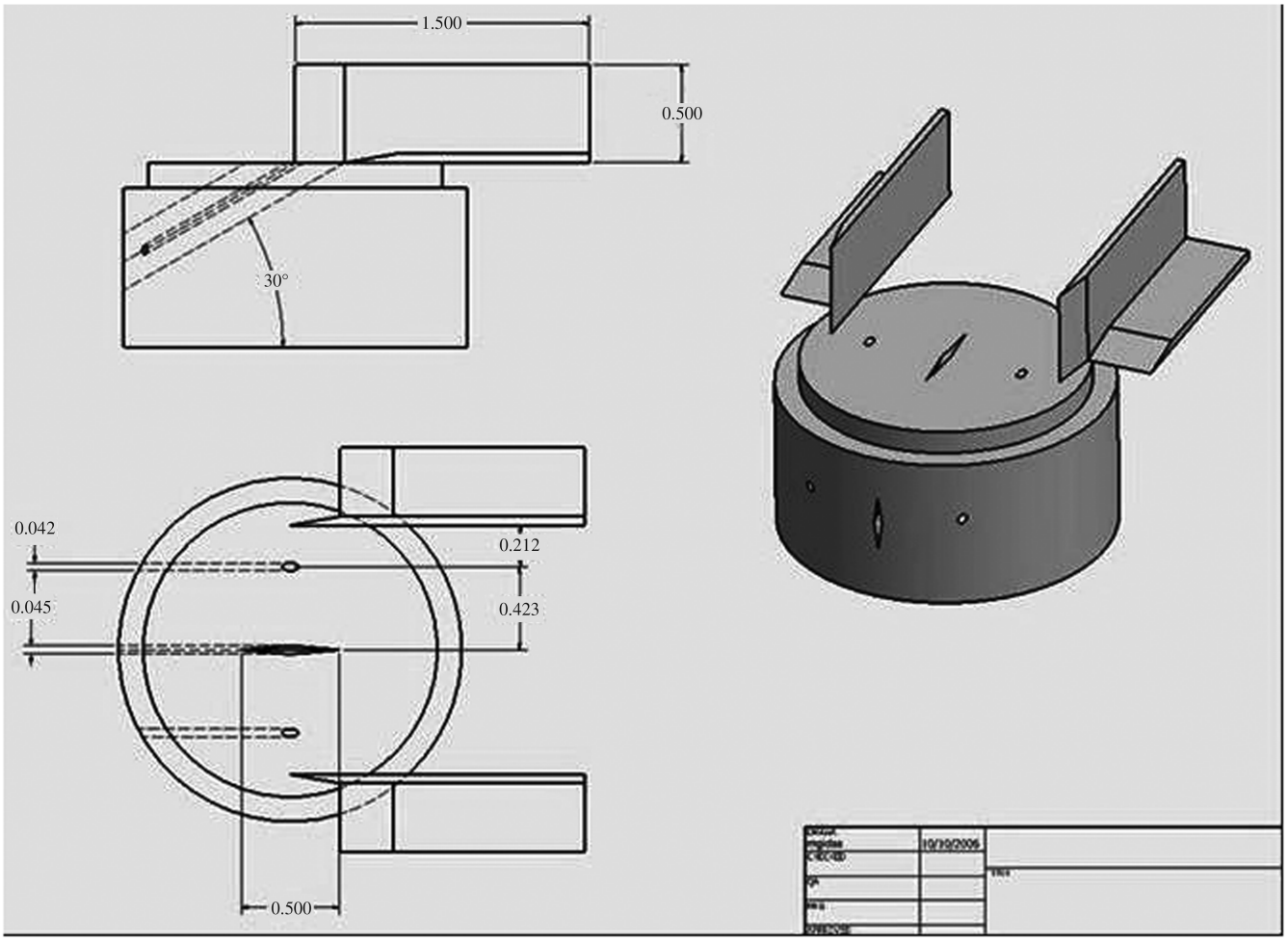

Fig. 3 Injector insert; dimensions are in inches.

because if $\bar{q}_{\text{diamond}}$ becomes too high, the jet can rapidly plume outward, losing the diamond shape and its benefits [14,27].

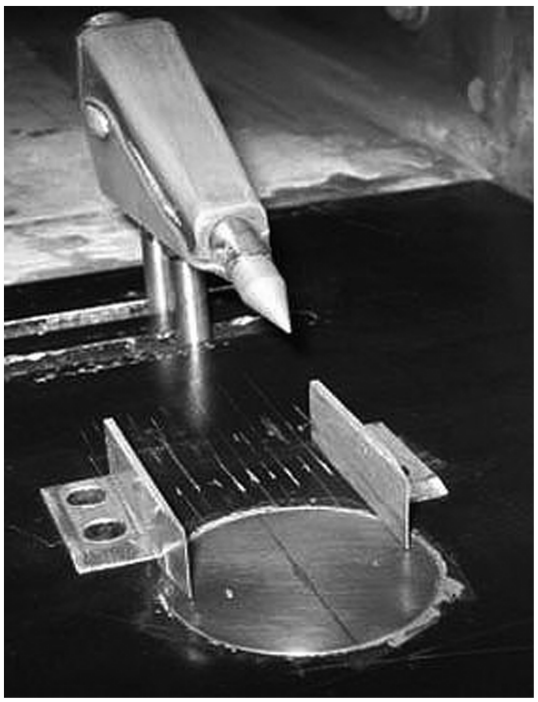

Fig. 4 Photograph of the injector insert mounted in the SST floor plate with the concentration probe behind.

D. Species Composition Probing

Mean helium-concentration measurements were accomplished using an integrated concentration sampling probe and gas analyzer designed for supersonic flow. The probe was aspirated during data acquisition by a vacuum pump. The conceptual design of this type of probe was originally developed by Ng et al. [28]. The concentration probe was calibrated to measure a unique helium mass fraction for a specific pressure, temperature, and heat transfer rate at the hot-film sensor plane. Complete details are available in [27]. The probe can be seen in Fig. 4.

A file was generated showing the probe position, voltage, total pressure, and total temperature for each wind-tunnel run. For each probe position, a computer algorithm using these measurements was used to determine the upper and lower bounds on voltage for any calibration level. The program then searched iteratively for the two helium-concentration calibration curves that bounded the voltage at the measured pressure and temperature. Then the local helium concentration was interpolated between the two bounding curves. These algorithms are shown in [27]. The probe was found to have an uncertainty of approximately ± 0.01 for helium mass fraction.

III. Computational Methods

A. Flow Solver

The flow solver used in all the simulations is the General Aerodynamic Simulation Program (GASP) [29] version 4.3. GASP is a time-dependent, three-dimensional, Reynolds-averaged Navier–Stokes (RANS) solver. It treats the integral form of the governing equations using upwind-based, finite volume formulations. GASP supports multiblock structured-grid topologies. In this study, the Euler implicit time-integration scheme was used with third-order

spatial accuracy for the convective fluxes and second-order accuracy for the diffusive fluxes.

The solutions were run in steady-state mode using a CFL based on the freestream velocity. The turbulence model was run uncoupled from the fluid equations. Running coupled versus uncoupled has more impact on convergence and CPU time than anything else. The final answer will be the same either way, but we find that running uncoupled is much faster. Both the fluid and turbulence time integration used a CFL value of 0.5 based on the freestream velocity.

B. Computational Region and Grid

The entire length of the computational grid was 10.2 cm. Of this, 1.27 cm was used to model upstream of the injectors and 7.6 cm was used downstream. The size of the computational domain was based on the experiment and available experimental data. The inflow was set at the location where the upstream boundary-layer thickness was measured. The downstream was set just aft of the measurements. The sides of the domain went out to the vertical splitter plates, and the top of the domain was set outside the influence of the jets. The diamond injector spanned 1.27 cm in the freestream direction. All injectors were modeled below the surface slightly to better simulate the jet interaction dynamics.

The grid was generated using the GridGen software package and consisted of 6,483,200 cells and 13 blocks (or zones). This was considered the fine grid from which the medium and coarse grids were created within GASP. The medium grid contained 810,400 cells and the coarse grid contained 101,300 cells. Mesh sequencing was used to help develop the flow and provide a good initial guess for the fine mesh. This involved running the CFD solver on the coarse grid until the solution was fairly converged. The solution was then interpolated to a medium grid and run until finally being interpolated to the fine grid. Mesh sequencing was also used to study grid convergence by comparing the solutions from the medium and fine grid levels. In previous numerical studies of jets in a high-speed crossflow [8], we have found that the values of the net forces on the surface are simple, effective indicators of grid convergence. For the present flow problem, the results of such a grid convergence study are shown in Table 1. We also looked at boundary-lay velocity profiles for the different grids. Taken together, these results were judged to demonstrate grid convergence for the fine grid.

Both the geometry and flow conditions allowed for the CFD simulation to be performed on half of the problem. Therefore, the grid was generated for half of the geometry and used a plane of symmetry. The symmetry plane for the medium grid for the inclined diamond injector is shown in Fig. 5, and the plane containing the surface is shown in Fig. 6. In Fig. 6, the grid near the symmetry plane through the inclined diamond injector can be seen at the top and the grid near the elliptical intersection of the inclined round injector can be seen below that. These types of flows are steady when run with a RANS solver. Similar types of flows have been run-time-accurate without assuming symmetry, to study the possibility of unsteadiness in the flow, but none was encountered. This problem was also run without a symmetry plane as a test. But, due to all the comparisons with various turbulence models, it was much more efficient to run half of the problem and take advantage of symmetry.

A hyperbolic tangent spacing was used to cluster points in the boundary layer such that a y^+ of around 1 was achieved for the first cell off the wall on the fine grid.

C. Boundary Conditions

For the surface, the no-slip adiabatic boundary condition was applied. The side wall (splitter plate) was modeled using the tangency condition. This essentially forced no flow through the surface with a slip-wall condition. This same condition was also applied to the symmetry plane.

Table 1 Grid convergence results

Grid designation	Tangent force, N	Normal force, N
Coarse	0.162	−18.34
Medium	0.154	−18.31
Fine	0.151	−18.31

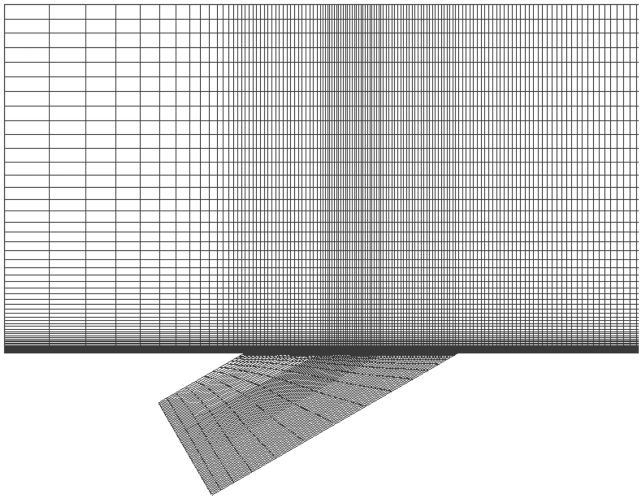

Fig. 5 Medium grid for the inclined diamond injector on the plane of symmetry.

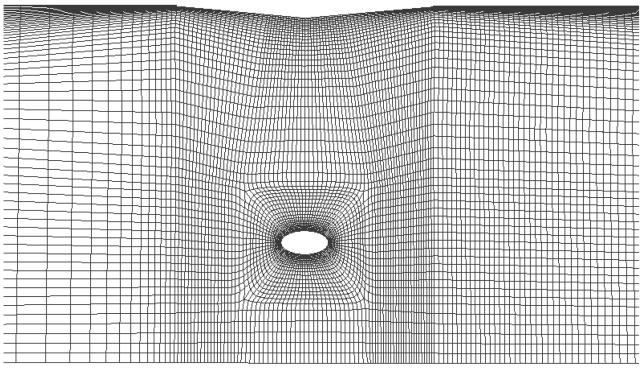

Fig. 6 Medium grid on the surface; inclined diamond injector on the plane of symmetry on the top, with the inclined circular injector below that.

For the inflow boundary, a pointwise boundary condition was used in which the flow conditions were held fixed. The profile for the inflow boundary was generated by running the tunnel conditions on a flat plate until the desired boundary-layer thickness was reached. From experiment, the boundary-layer thickness was known to be 17 mm just upstream of the injectors. The outflow boundary, as well as the top surface, used the extrapolation condition. For the injectors, a fixed inflow boundary condition was applied. The flow conditions were set to match the experimental mass flow and a sonic velocity. The inflow condition to the injectors were set to constant values. This boundary condition for the injectors was not at the surface of the plate, but upstream inside the ducts (see Fig. 5). A boundary layer did form by the time the flow reached the nozzle exit. Because the actual profile was unknown upstream in each duct, the focus was placed on trying to match the mass flow and the sonic condition at the duct exit.

D. Turbulence Models

The baseline turbulence model used was Wilcox's k-ω model [30] (1998 version). The selection for this two-equation model came from research by Viti et al. [8]. The Wilcox k-ω model tends to be more accurate for boundary layers with adverse pressure gradients when compared with other one- and two-equation models. The k-ω model does not require wall functions and does an adequate job for various types of free shear flows. To study the sensitivity of the CFD predictions to the choice of turbulence model, additional tests were run with the following range of well-known models: 1) the

one-equation Spalart–Allmaras model [31], 2) Menter's two-equation shear stress transport (SST) model [32], and 3) Wilcox's seven-equation Reynolds stress model (RSM) [30]. This group of models spans a wide range of the types commonly applied in the CFD field. All turbulence models were run with a compressibility correction. When mixing occurs in supersonic flows, a correction to most all turbulence models is necessary to account for the reduced mixing rates. For the GASP code, this was detailed in [33].

IV. Results

The main experimental measurements were helium mass fraction contours in a cross plane at 3.71 cm downstream from the center of the injectors. This corresponds to $x/d_{\text{eff}} = 34.5$ and $x/R_b = 33.5$. In the plots that follow, the vertical and horizontal scales are nondimensionalized by the effective diameter. Results are shown in Fig. 7. Note the substantially higher penetration of the center diamond injector plume, compared with the circular injector plumes on either side. The increase in penetration of the plume from the diamond injector, compared with those for the circular injectors, can be seen to be at least a factor of 2, which is more than from the tests comparing isolated diamond and circular injectors, where a factor of about 1.5 has been reported [13,28]. One can presume that this improved performance is a result of favorable interference in the array. The rate of mixing is about the same, as indicated by the maximum concentration levels in the plumes for the circular and diamond injectors.

The CFD prediction using Wilcox's k-ω model is shown in Fig. 8 with the same grayscale shading as the experiment. The maximum concentrations are approximately the same for the diamond injector, yet the experiment shows higher concentrations for the circular injectors. The CFD solution predicts the penetration height of the diamond injector to be slightly less than that of the experiment. For the circular injectors, the penetration height comparison is roughly the same. Note that the experiment shows some differences here between the left and right circular injectors.

The CFD solution also shows no mixing between the diamond and circular injectors at the given location of the experimental data. In the experiment, the helium concentrations show some overlap of the plumes.

A plot showing the predicted velocity vectors from the diamond and circular jets is given in Fig. 9. Here, the vortex structures of the diamond- and circular-jet plumes are evident. The vectors are shaded to velocity magnitude. The counter-rotating vortices from the circular injector tend to trap more of the helium, as shown in Fig. 8, with the higher He concentration at the vortex centers.

To better visualize the flowfield, stream traces from both injectors were created and shown in Fig. 10. Here, the traces are shaded to the

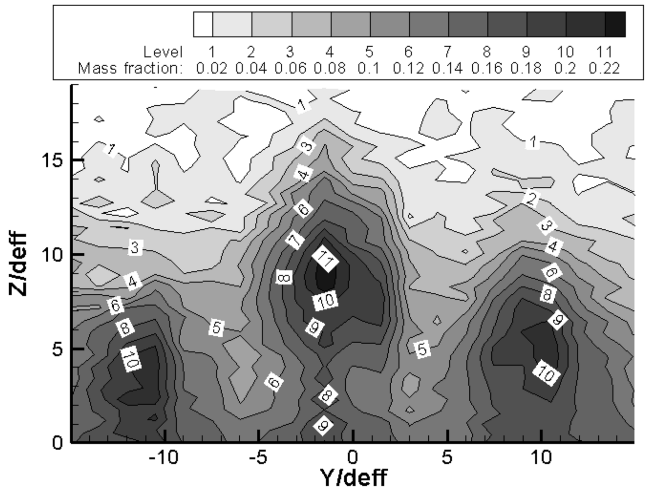

Fig. 7 Experimental helium mass fraction contours at $x/d_{\text{eff}} = 34.5$ and $x/R_b = 33.5$.

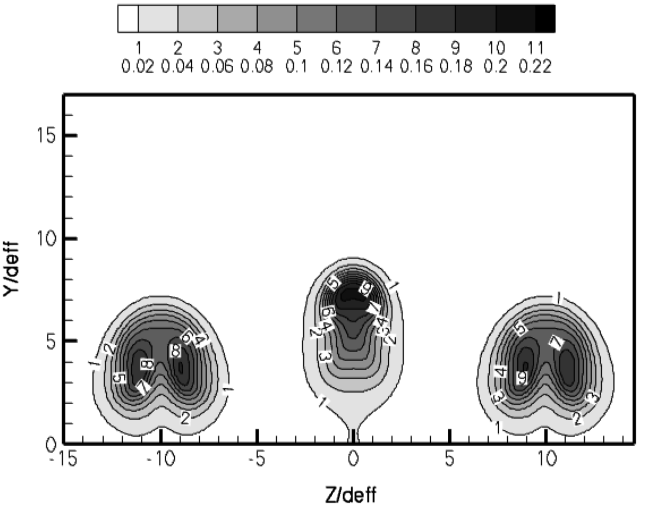

Fig. 8 CFD prediction of He mass fraction contours at $x/d_{\text{eff}} = 34.5$ and $x/R_b = 33.5$ using Wilcox's k-ω model.

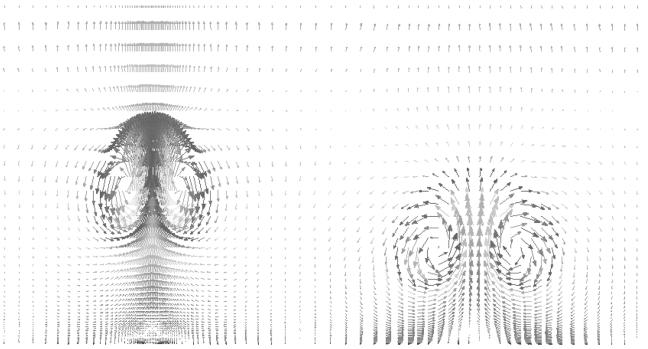

Fig. 9 CFD prediction of vortex structures in the plumes at $x/d_{\text{eff}} = 34.5$ and $x/R_b = 33.5$; diamond (left) and circular jet (right).

He concentrations using the same legend as Fig. 8. In addition to the stream traces, the pressure field on the plate is shown. For the diamond injector, the stream traces originate from a line source through the middle of the injector. The flow from the center of the diamond disperses very little as it swirls downstream and forms the peak concentration at x/d_{eff} of 34.5. Traces from the forward and aft

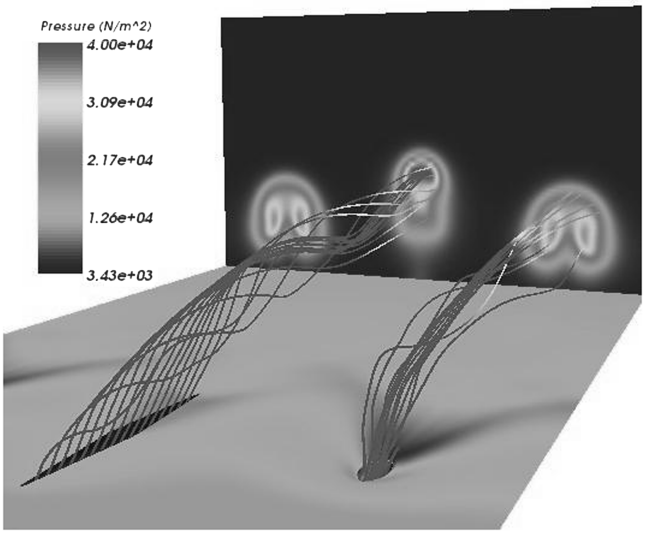

Fig. 10 Stream traces of He from the injectors along with pressure contours on the plate (He legend is the same as in Fig. 8).

Fig. 11 Centerline slice of each injector showing He concentration (He legend is the same as in Fig. 8); diamond injector (left) and circular injector (right).

parts of the injector (near the diamond tips) tend to mix more with the incoming flow.

Stream traces from the circular injector show that helium from the center tends to follow a more parabolic line, meaning that it escapes from being entrained by the vortices that form. Helium from the center of the injector appears to propagate more toward the top of the He concentration profiles, as seen in Fig. 10. The helium that gets entrained in the vortex structures originates more from the flow exiting near the injector sides.

The pressure on the plate surface shows a lower pressure region behind the circular injector, compared with the diamond injector. There is also a higher pressure in front of the circular injector, due to a stronger shock that forms there. The interaction of each injector with the incoming flow is very different, and it is this combination that gives hope to producing better mixing for high-speed combustion applications.

A streamwise slice through the center of each injector is shown in Fig. 11. The helium concentration is shown with the same grayscale contour levels as given in Fig. 8. The location of the experimental data is indicated by a vertical line on each plot.

To see the impact that the turbulence model selection has on the CFD results, several other models were used to generate solutions. The other models were the one-equation Spalart–Allmaras model, the two-equation SST model by Menter, and a seven-equation RSM by Wilcox. In most RANS simulations involving turbulence, the appropriate selection of the turbulence model can be critical. Given the complex flow structure in the current simulation, it is very likely that the turbulence model contributes the highest uncertainty in the results. For this reason, running the simulation using various turbulence models helps one gauge the uncertainties and deficiencies in turbulence modeling.

The predicted helium concentration using the Spalart–Allmaras model is compared with the baseline Wilcox k-ω model in Fig. 12. Here, the Wilcox model prediction is shown on the left and the Spalart–Allmaras model prediction is on the right. On the fine grid, the maximum He concentrations were 0.21 for Wilcox's model and only 0.08 for the Spalart–Allmaras model. The predicted level of mixing is much greater for the Spalart–Allmaras model and would not appear to be a good choice for the current problem.

The same comparison for Menter's SST model is shown in Fig. 13. Here, the maximum He concentration for the SST model is 0.14. Although the SST model uses the same independent variables as the Wilcox k-ω model, the mixing that each model predicts is quite different. The last comparison is made between the baseline model and a RSM, also by Wilcox, as shown in Fig. 14. In theory, the RSM model should be better equipped to handle three-dimensional separated flows with mixing. The maximum concentration of the RSM model at x/d_{eff} of 34.5 is 0.18, just slightly less than the 0.21 of the baseline model. The one improvement of the RSM prediction

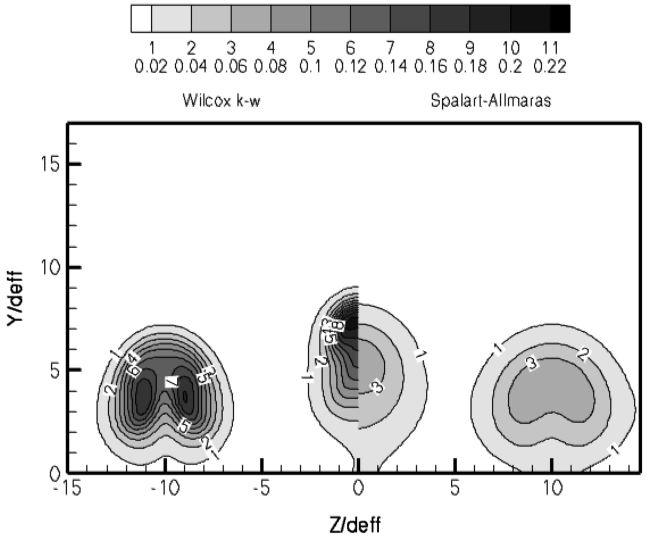

Fig. 12 CFD predictions of He mass fraction contours at $x/d_{\text{eff}} = 34.5$ and $x/R_b = 33.5$ with Wilcox k-ω and Spalart–Allmaras turbulence models.

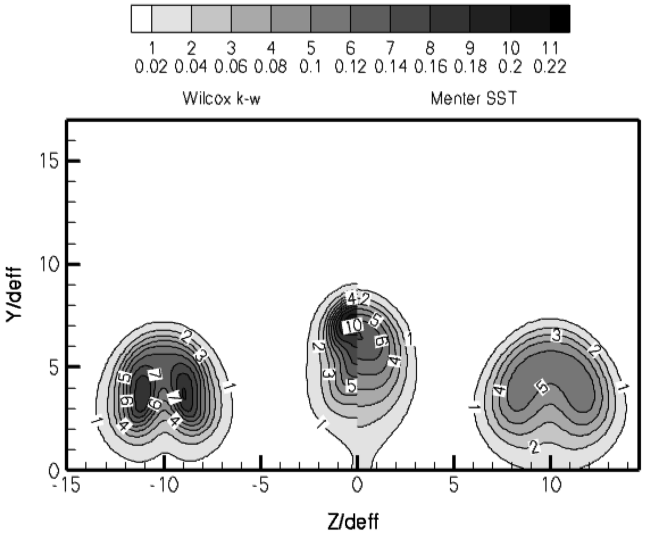

Fig. 13 CFD predictions of He mass fraction contours at $x/d_{\text{eff}} = 34.5$ and $x/R_b = 33.5$ with Wilcox k-ω and Menter's SST turbulence models.

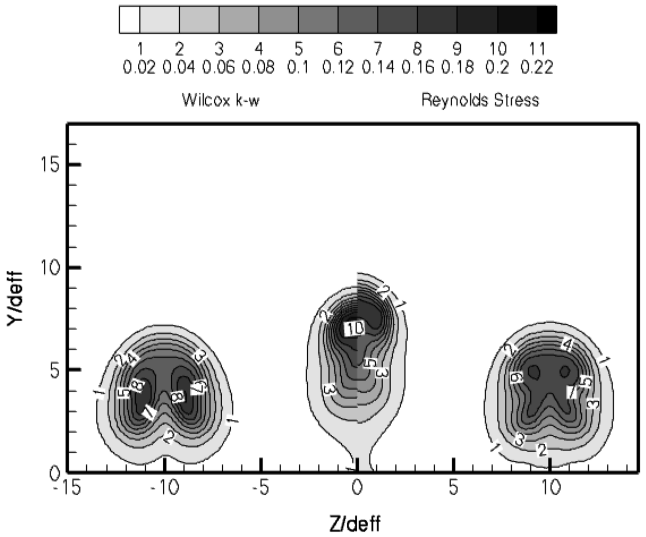

Fig. 14 CFD predictions of He mass fraction contours at $x/d_{\text{eff}} = 34.5$ and $x/R_b = 33.5$ with Wilcox k-ω and Reynolds stress models.

over the baseline is a slightly greater penetration of the diamond injector into the flow.

Looking over the helium-mixing predictions from the four turbulence models, the simulations are heavily impacted by the turbulence model selection. None of the turbulence models were able to accurately simulate the helium mixing shown in the experiment, but some models did much better than others. From the four models considered here, the k-ω model by Wilcox had the best correlation with the experimental helium-concentration profiles.

V. Conclusions

This paper presented the results of experimental and numerical studies of an array of injectors combining inclined circular and diamond-shaped sonic nozzles for application to high-Mach-number vehicles with light-gas fuels. The freestream Mach number was 4, and helium was used as the injectant to safely simulate hydrogen fuel. The diamond injector provided improvements in penetration of more than a factor of 2, compared with circular injectors. This is a considerably greater increase than had been inferred earlier by comparing test results with isolated diamond and circular injectors. The implication is that there is a synergistic effect when these kinds of injectors are combined into an array. The rate of mixing, as indicated by the level of maximum injectant concentration in the plume, was about the same for the circular and diamond injectors.

CFD with a RANS formulation was able to provide good simulations of penetration and reasonable predictions of mixing with the Wilcox k-ω turbulence model. Both the Spalart–Allmaras model and Menter's SST model overpredicted the rate of mixing. The Wilcox Reynolds stress model predicted a slightly greater penetration of the diamond injector into the flow, but also overpredicted the mixing to some degree. Overall, the Wilcox k-ω turbulence model provided the best predictions. The solution with that model was probed in detail to highlight the differences in the flow in the plumes from the circular and diamond injectors.

An important objective of a cold-flow mixing study such as conducted here is to quantify the uncertainty of CFD predictions for such an injector design so that the reliability of CFD predictions for hot-flow combusting conditions can be judged. Detailed experimental flowfield studies are extremely challenging under the hot-flow conditions of interest for Mach 10 vehicles, and so the combustor designer must rely on CFD. Based on the results obtained in this study, one must conclude that CFD predictions for complex flows such as these have a rather large uncertainty.

From a combustor design point of view, these results show that it is useful to combine inclined diamond and circular injectors to achieve good fuel coverage and fuel/air mixing across a combustor.

Acknowledgment

This work was supported primarily by a U.S. Air Force Office of Scientific Research (AFOSR) Multidisciplinary University Research Initiative (MURI) led by Paul Dimotakis at California Institute of Technology.

References

[1] Maddalena, L., Campioli, T. L., and Schetz, J. A., "Experimental and Computational Investigation of an Aeroramp Injector in a Mach Four Cross Flow," AIAA/CIRA 13th International Space Planes and Hypersonics Systems and Technologies, AIAA Paper 2005-3235, June 2005.

[2] Hartfield, R. J., Hollo, S. D., and McDaniel, J. C., "Experimental Investigation of a Supersonic Swept Ramp Injector Using Laser Induced Iodine Fluorescence," *Journal of Propulsion and Power*, Vol. 10, No. 1, Jan.–Feb. 1994, pp. 129–135.

[3] Doerner, S. E., and Cutler, A. D., "Effects of Jet Swirl on Mixing of a Light Gas Jet in a Supersonic Airstream," NASA CR-1999-209842, Dec. 1999.

[4] Schetz, J. A., Cox-Stouffer, S., and Fuller, R., "Integrated CFD and Experimental Studies of Complex Injectors in Supersonic Flows," AIAA Paper 98-2780, June 1998.

[5] Jacobsen, L. S., Gallimore, S. D., Schetz, J. A., and O'Brien, W. F., "Integration of an Aeroramp Injector/Plasma Igniter for Hydrocarbon Scramjets," *Journal of Propulsion and Power*, Vol. 19, No. 2, Mar.–Apr. 2003, pp. 170–182.

[6] Fuller, R. P., Wu, P. K., Nejad, A. S., and Schetz, J. A., "Comparison of Physical and Aerodynamic Ramps as Fuel Injectors in Supersonic Flow," *Journal of Propulsion and Power*, Vol. 14, No. 2, Mar.–Apr. 1998, pp. 135–145.

[7] Jacobsen, L. S., Gallimore, S. D., Schetz, J. A., O'Brien, W. F., and Goss, L. P., "Improved Aerodynamic-Ramp Injector in Supersonic Flow," *Journal of Propulsion and Power*, Vol. 19, No. 4, July–Aug. 2003, pp. 663–673.

[8] Viti, V., Schetz, J. A., and Neel, R., "Numerical Studies of the Jet Interaction Flowfield with a Main Jet and an Array of Smaller Jets," International Council of the Aeronautical Sciences Paper 2002-4.7.1, 2002.

[9] Schetz, J. A., Cox-Stouffer, S., and Fuller, R., "Integrated CFD and Experimental Studies of Complex Injectors in Supersonic Flows," AIAA Paper 98-2780, 1998.

[10] Riggins, D. W., and Vitt, P. H., "Vortex Generation and Mixing in Three-Dimensional Supersonic Combustors," *Journal of Propulsion and Power*, Vol. 11, No. 3, May–June 1995, pp. 419–426.

[11] Lewis, D. P., and Schetz, J. A., "Tangential Injection from Overlaid Slots into a Supersonic Stream," *Journal of Propulsion and Power*, Vol. 13, No. 1, Jan.–Feb. 1997, pp. 59–63.

[12] Schetz, J. A., Billig, F. S., Favin, S., and Gilreath, H. E., "Effects of Pressure Mismatch on Slot Injection in a Supersonic Flow," *International Journal of Turbo and Jet Engines*, Vol. 9, No. 2, 1992, pp. 135–146.

[13] Barber, M. J., Schetz, J. A., and Roe, L. A., "Normal Sonic Helium Injection Through a Wedge-Shaped Orifice into a Supersonic Flow," *Journal of Propulsion and Power*, Vol. 13, No. 2, Mar.–Apr. 1997, pp. 257–263.

[14] Tomioka, S., Jacobsen, L. S., and Schetz, J. A., "Sonic Injection from Diamond-Shaped Orifices into a Supersonic Crossflow," *Journal of Propulsion and Power*, Vol. 19, No. 1, Jan.–Feb. 2003, pp. 104–114.

[15] Schetz, J. A., "Interaction Shock Shape for Transverse Injection," *Journal of Spacecraft and Rockets*, Vol. 7, No. 2, Feb. 1970, pp. 143–149.

[16] Fuller, E. J., Mays, R. B., Thomas, R. H., and Schetz, J. A., "Mixing Studies of Helium in Air at Mach 6," AIAA Paper 91-2268, June 1991.

[17] McClinton, C. R., "The Effect of Injection Angle on the Interaction Between Sonic Secondary Jets and a Supersonic Freestream," NASA TND-6669, Feb. 1972.

[18] Rogers, R. C., "A Study of the Mixing of Hydrogen Injected Normal to a Supersonic Airstream," NASA Langley Research Center TN L-7386, Hampton, VA, Mar. 1971.

[19] Jacobsen, L. J., Schetz, J. A., Gallimore, S. D., and O'Brian, W. F., "Mixing Enhancement by Jet Swirl in a Multiport Injector Array in Supersonic Flow," Fluids Engineering Div. Summer Meeting American Society of Mechanical Engineers Paper 99-7448, July 1999.

[20] Kraus, D. K., and Cutler, A. D., "Mixing of Swirling Jets in a Supersonic Duct Flow," *Journal of Propulsion and Power*, Vol. 12, No. 1, Jan.–Feb. 1996, pp. 170–177.

[21] Cutler, A. D., and Johnson, C. H., "The Use of Swirling Jet Pairs to Provide Rapid Fuel Penetration in Scramjet Combustors," AIAA Paper 95-0099, 1995.

[22] Schetz, J. A., *Injection and Mixing in a Turbulent Flow*, AIAA, New York, 1980.

[23] Povinelli, L. A., and Ehlers, R. C., "Swirling Base Injection for Supersonic Combustion Ramjets," *AIAA Journal*, Vol. 10, No. 9, Sept. 1972, pp. 1243–1244.

[24] Schetz, J. A., and Swanson, R. C., "Turbulent Jet Mixing at High Supersonic Speeds," *Zeitschrift fur Flugwissenschaften und Weltraumforschung*, Vol. 21, 1973, pp. 166–173.

[25] Schetz, J. A., Thomas, R. H., and Billig, F. S., "Mixing of Transverse Jets and Wall Jets in Supersonic Flow," *IUTAM Symposium on Separated Flows and Jets*, Springer–Verlag, Berlin, 1990.

[26] Marzouk, Y. M., and Ghoniem, A. F., "Mechanism of Streamwise Vorticity Formation in Transverse Jets," 40th AIAA Aerospace Sciences Meeting and Exhibit, Reno, NV, AIAA Paper 2002-1063, Jan. 2002.

[27] Grossman, P., Maddalena, L., and Schetz, J., "Flush-wall, Diamond-shaped Fuel Injector for High Mach Number Scramjets," *Journal of Propulsion and Power*, Vol. 24, No. 2, 2008, pp. 259–266. doi:10.2514/1.29956

[28] Ng, W. F., Kwok, F. T., and Ninnemann, T. A., "A Concentration Probe for the Study of Mixing in Supersonic Shear Flows," AIAA Paper 89-2459, July 1989.

[29] GASP, Software Package, Ver. 4.0, AeroSoft, Blacksburg, VA, 2002.

[30] Wilcox, D. C., *Turbulence Modeling for CFD*, 2nd ed., DCW Industries, La Cañada, CA, 1998.
[31] Spalart, P. R., and Allmaras, S. R., "A One Equation Turbulence Model for Aerodynamic Flows," *La Recherche Aérospatiale: Bulletin Bimestriel de l'Office National d'Études et de Recherches Aérospatiales*, No. 1, 1994, pp. 5–21.
[32] Menter, F. R., "Zonal Two Equation k-ω Turbulence Models for Aerodynamic Flows," AIAA Paper 93-2906, July 1993.
[33] Neel, R., Godfrey, A., and Slack, D., "Turbulence Model Validation in GASP Version 4," AIAA Paper 2003-3740, June 2003.

K. Frendi
Associate Editor